electronics

MDPI

Article

Magnetic Characterization of MR Fluid by Means of Neural Networks

Paweł Kowol [1], Grazia Lo Sciuto [1,2], Rafał Brociek [3,*] and Giacomo Capizzi [2,3]

[1] Department of Mechatronics, Silesian University of Technology, Akademicka 2A, 44-100 Gliwice, Poland; pawel.kowol@polsl.pl (P.K.); grazia.losciuto@polsl.pl (G.L.S.)
[2] Department of Electrical, Electronics and Informatics Engineering, University of Catania, Viale Andrea Doria 6, 95125 Catania, Italy; giacomo.capizzi@unict.it
[3] Department of Mathematics Applications and Methods for Artificial Intelligence, Faculty of Applied Mathematics, Silesian University of Technology, 44-100 Gliwice, Poland
* Correspondence: rafal.brociek@polsl.pl

Abstract: Magnetorheological and electrorheological fluids manifest a change in rheological behavior when subjected to a magnetic or electric field, respectively, such that they require electrical and magnetic characterization. In this paper, a simple and accurate mathematical model based on a small number of parameters provides the relative magnetic permeability of magnetorheological fluids as a function of the applied magnetic field. Furthermore, for the testing and magnetic characterization of magnetorheological fluids, a new metering equipment setup is implemented. Starting with the achieved experimental data, the mathematical relation $\mu_r = f(B)$ is represented by means of a radial basis function neural network, with neurons having a Gaussian activation function; by means of post-training pruning procedures, the trained neural network is applied using the proposed data. Therefore, the obtained mathematical relation $\mu_r = f(B)$ is in good agreement with the experimental data, with an approximate error of 8%.

Keywords: Gabor system; MR fluids; radial basis function neural network; relative magnetic permeability

check for updates

Citation: Kowol, P.; Lo Sciuto, G.; Brociek, R.; Capizzi, G. Magnetic Characterization of MR Fluid by Means of Neural Networks. *Electronics* **2024**, *13*, 1723. https://doi.org/10.3390/electronics13091723

Received: 19 March 2024
Revised: 24 April 2024
Accepted: 26 April 2024
Published: 29 April 2024

1. Introduction

In the last few years, the advances in materials technology and the important role of electronics in mechanical engineering have yielded significant progress in the production of electric vehicles and in the automotive industries. Variable-friction dampers, clutches, brakes, shock absorbers and hydraulic valves are used mainly in heavy industry, with applications such as heavy motors and heavy duty trucks, exploiting smart materials [1].

Smart materials are materials created in a laboratory that react to different external stimuli and respond to changes in their environment. Metals that react to high temperatures by modifying their structures and assuming a predictable shape are called smart materials, responding in a pre-determined manner to temperature variations. An example of a smart material is nickel titanium, also known as Nitinol, or a metal alloy of nickel and titanium, that changes shape when immersed in liquids at a high temperature. Shape memory materials are particular polymeric smart materials that change their shape, assuming a different one if subjected to an external stimulus such as a high temperature. In addition, smart materials can transform and change their structures when subjected to physical stress or exposed to electric and magnetic fields or light. An interesting application of these materials is their use in so-called intelligent systems (smart systems or smart structures). Magnetorheological (MR) and electrorheological (ER) fluids are materials that manifest a change in rheological behavior when subjected, respectively, to a magnetic or electric field [2–4].

The rheological variation is reversible, ceasing when the external field is removed for milliseconds. The electrorheological phenomenon is also called the Winslow effect. ER and MR fluids are known as controllable fluids (CF) due to the possibility to develop precise characteristics that are controllable in the rheological response. Controllable fluid technology has seen a long initial stage. The relatively low strength and temperature, contaminant sensitivity and the necessity of high voltages for ER fluids have impeded their widespread commercialization, as reported in [5,6]. Recently, the importance of these materials has been demonstrated in defining the interface between the electrical system and mechanics. MR liquids have applications in the mechanical (dampers, decelerators), automotive and aerospace (suspension, brakes, clutches), biomedical (dampers for prostheses) and construction industries (supports seismic) [7–10]. The advantage of MR materials compared to traditional materials is the ability to obtain damping without the need to vary the cross-sectional area, since the itself fluid controls the damping through a change in its viscosity. Another important application of MR is the biomedical one, with the use of prosthetic devices suitable for improving the movement of the knees in limb amputees in whom a prosthesis has been applied. Because of their high precision and control speed (the time of response is less than 10 milliseconds), these fluids allow us to obtain exceptional results concerning the fluidity and spontaneity of movement articulation [11,12]. MR fluids are composed of water and mineral, synthetic or silicone oils mixed with 10–40% of dispersed iron powder with a size of 0.1–10 µm. In an inactive state, MR fluids react as typical natural oils in Newtonian liquids. Applying an external magnetic field through the fluid, MR fluids are activated, causing the micron-sized particles to form magnetic dipoles along the magnetic lines of force and increasing the viscous resistance with non-Newtonian Fluid behavior [13,14]. Consequently, MR fluids can change from a liquid to a solid state under the influence of a magnetic field [15]. MR fluids can tolerate shear stress until a yield stress threshold, strongly depending on the strength of the applied magnetic field and due to the chains' resistance against flow [16,17]. The control of the physical change of the MR fluid from liquid to semi-solid under the application of a magnetic field is useful for active vibration control and brakes [18]. Thus, the magnetic property of MR materials cannot be represented by a constant relative magnetic permeability [19]. Therefore, methods for the measurement of the permeability of fluids under different values of magnetization, temperature and frequency are crucial in many applications for industrial utilization [20,21]. For the description of complicated MR fluids' physical properties, the models recently considered in the literature, based on a large number of technical parameters, are able to reproduce some of their aspects.

Within this framework, the authors propose an experimental measurement MR device and a mathematical model to characterize MR fluids (Figure 1).

The main contributions of this work are as follows.

- A measurement device is designed and realized for the characterization of MR fluids.
- The MR device exhibits a magnetic response to electrical stimuli. Measurements of the magnetic permeability (μ_r) and magnetic field intensity (B) have been conducted in the complex configuration of the MR fluid device.
- An advanced radial basis function neural network (RBF) with a Gaussian activation function is developed to relate the relative magnetic permeability and magnetic field intensity of MR fluids.

The simple and accurate mathematical model, based on a small number of parameters, provides the relative magnetic permeability of the MR fluid as a function of the applied magnetic field. The mathematical function model defined as $\mu_r = f(B)$ is a compact analytical expression approximated by the linear combination of the elements of a *Gabor* system, achieved by the translation and scaling of the Gaussian function $\phi(t) = e^{-t^2}$. The Gaussian function is preferred for its rapid decay and for the approximation of complex mathematical relationships with few non-zero coefficients. The Gabor system forms a frame [22]. The reconstruction of a function f from its frame coefficients can be calculated with a pseudo-inverse operator, but, often, this operator is not necessarily bounded. The latter induces numerical instabilities when trying to reconstruct f from its frame coefficients. To achieve the highly efficient reconstruction of the function and implement the mathematical expression of $\mu_r = f(B)$, the proposed method uses a radial basis function neural network (RBF) with a Gaussian activation function [23,24]. The network is trained with experimental data and a pruning procedure is applied [25,26]. Therefore, the obtained mathematical relation $\mu_r = f(B)$ is in good agreement with the experimental data, with an approximate error of 8%.

Figure 1. Experimental set-up.

The mathematical methodology based on RBF has demonstrated advantages in terms of efficiency, processing speed and generalization compared to the existing models of the dependence of the magnetic field and MR magnetic permeability in the device, with great potential in industrial engineering. Comparisons of the numerical results and experimental data with this approach could be useful in the design of new MR devices. However, the model needs to be developed not only in the laboratory but for practical engineering applications, including new parameters and expanding the dataset of the device's geometry. In future work, studies could be focused on the construction of a new device in conjunction with the industry and the validation of the mathematical model.

The paper is structured as follows. Section 2 discusses previous research works. Section 3 introduces the theoretical concepts of the RBFN and MR fluids. Section 4 describes the experimental set-up and measurements conducted in the laboratory; the results and neural modeling are discussed in Section 5. Finally, Section 6 closes the paper with the conclusions.

2. Related Works

Radial basis function (RBF) networks are used for function approximation problems in various applications, including function approximation, time series prediction, classification tasks and control [27,28]. This type of artificial neural network uses radial basis functions as activation functions, and it consists of an input layer, a hidden layer and an output layer [29]. The hidden layer applies the radial basis function, typically a Gaussian function [30]. RBF networks are computational models used for their simple architecture, fast training speed and the opportunity to include real data in the system. In the analysis of the magnetohydrodynamics of a Ree–Eyring fluid, the effect of the Hall current between two parallel plates was numerically solved by using radial basis functions [31].

Due to the nonlinear characteristics of magnetorheological dampers and magnetorheological elastomer-based isolators, the approximation of the forward and inverse dynamic behaviours was performed using radial basis function (RBF) networks in [32,33]. Therefore, different theoretical models have been investigated, such as the Maxwell–Garnett mixing rule, applicable to the calculation of the effective permeability and the average magnetic field of the between adjacent particles and the continuous phase in MRF [34]. A mathematical expression of the magnetic flux density was established to assess the behaviour of compression and shear after the squeezing of MR fluids, which was simulated and compared using finite element analysis in [35]. A computational fluid dynamics model of a magnetorheological (MR) fluid operated in squeeze mode with a constant interface area was presented in [36–38].

In this paper, an RBF network with a Gaussian activation function was developed to relate the magnetic permeability of MR fluids and the magnetic field applied in the measuring device.

3. Theoretical Background

3.1. Radial Basis Function

The radial basis function (RBFN) was derived from the traditional interpolation problem [39,40]. The RBFN has three layers as input, a hidden layer and a linear output. It is considered one of the best solutions to the real multi-variable interpolation problem for data that are not uniformly sampled. RBF neural networks have only one hidden layer and an activation function based on a Gaussian function as a radial basis function. The learning algorithm in RBFNNs is linear and fast, able to represent complex nonlinear input–output mapping. This network employs a linear combination of radially symmetric functions. Mathematically, this problem can be stated as follows.

Given n different points $\{\mathbf{x}_i \in \mathbb{R}^p, i = 1, 2, \ldots, n\}$ *and n real numbers,* $\{y_i \in \mathbb{R}, i = 1, 2, \ldots, n\}$*, find a function* $f : \mathbb{R}^p \longrightarrow \mathbb{R}$ *such that the following interpolation conditions are satisfied:*

$$f(\mathbf{x}_i) = y_i, \quad i = 1, 2, \ldots, n \tag{1}$$

The radial basis function (RBF) expansion, given in the following equation, can be used to solve this problem in a very efficient way. The RBF is a function whose value depends on the Euclidean distance to a center x_i in the input space as the Gaussian RBF.

$$y = f(\mathbf{x}) = \sum_{i=1}^{n} w_i \phi(\|\mathbf{x} - \mathbf{x}_i\|) \tag{2}$$

where x, $y(x)$, x_i and w_i are, respectively, the input, output, center and weights. In Equation (2), ϕ is the activation function and $\|\mathbf{x} - \mathbf{x}_i\|$ is the Euclidean distance between x and x_i.

Then, the interpolation conditions of Equation (1) can be interpreted as

$$\begin{bmatrix} \phi_{1,1} & \phi_{1,2} & \cdots & \phi_{1,n} \\ \phi_{2,1} & \phi_{2,2} & \cdots & \phi_{2,n} \\ \vdots & \vdots & \ddots & \vdots \\ \phi_{n,1} & \phi_{n,2} & \cdots & \phi_{n,n} \end{bmatrix} \begin{bmatrix} w_1 \\ w_2 \\ \vdots \\ w_n \end{bmatrix} = \begin{bmatrix} y_1 \\ y_2 \\ \vdots \\ y_n \end{bmatrix} \tag{3}$$

with

$$\phi_{i,j} \triangleq \phi(\|\mathbf{x}_j - \mathbf{x}_i\|) \quad i, j = 1, 2, \ldots, n$$

if the output y and weights w are set as

$$\mathbf{y} = \begin{bmatrix} y_1 \\ y_2 \\ \vdots \\ y_n \end{bmatrix} \in \mathbb{R}^n, \quad \mathbf{w} = \begin{bmatrix} w_1 \\ w_2 \\ \vdots \\ w_n \end{bmatrix} \in \mathbb{R}^n$$

and

$$\mathbf{\Phi} = \begin{bmatrix} \phi_{1,1} & \phi_{1,2} & \cdots & \phi_{1,n} \\ \phi_{2,1} & \phi_{2,2} & \cdots & \phi_{2,n} \\ \vdots & \vdots & \ddots & \vdots \\ \phi_{n,1} & \phi_{n,2} & \cdots & \phi_{n,n} \end{bmatrix}$$

Then, Equation (2) can be expressed in a compact way as

$$\mathbf{\Phi w} = \mathbf{y} \tag{4}$$

A necessary and sufficient condition to solve the interpolation problem is the invertibility of the matrix $\mathbf{\Phi}$. Hence, if it is possible to select the radial basis function $\phi(.)$ such that $\mathbf{\Phi}$ is non-singular, then the solution of the weight vector $\mathbf{w}$ is obtained as

$$\mathbf{w} = \mathbf{\Phi}^{-1}\mathbf{y} \tag{5}$$

In [41], for n distinct points $\mathbf{x_1}, \mathbf{x_2}, \cdots, \mathbf{x_n} \in \mathbb{R}$, the non-singularity of $\mathbf{\Phi}$ can be guaranteed by the Gaussian radial basis function

$$\phi(t) = e^{-(r/\sigma)^2} \tag{6}$$

In Equation (6), r and σ are the centers and widths, respectively. The training procedure of the RBF network involves the grouping of the training patterns and the computation of the RBF activation functions for the training inputs (Equation (2)) and weights by least squares. A typical RBF neural network is constituted by three layers, with an input layer, an intermediate layer of Gaussian units (neurons with Gaussian activation functions) and an output stage of conventional summation units. A block diagram showing the input–output of the Gaussian RBF is shown in Figure 2.

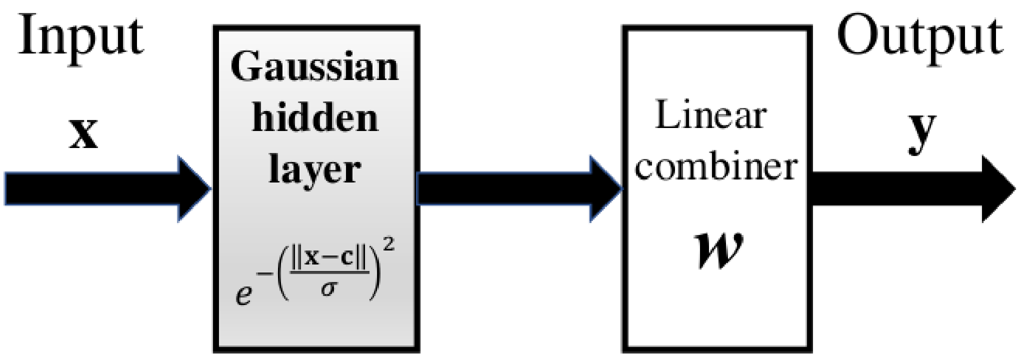

Figure 2. A block diagram of an RBF neural network.

Different approaches are presented to train RBF neural networks; some approaches are supervised while others are unsupervised and some are mixed, where the centroids and weights can be calculated at the same time or can be determined independently of each other. Thus, a supervised training method can be used for the weights and an unsupervised method for the centroids, or vice versa.

The most commonly used approach is the mixed one: first, the center and variance parameters are determined, followed by the learning or adjustment of the weight parameters of the linear combinators in the output layer [42].

3.2. Magnetorheological Fluids

The physical and mechanical properties of MR fluids are directly controlled to obtain solid magnetic characteristics under the operating temperature. However, the MR fluid behaves as a typical Newtonian fluid in the absence of an externally applied magnetic field.

The schematic of the MR fluid is presented in Figure 3, providing three main components:

- A liquid carrier;
- Ferromagnetic particles;
- A non-magnetic surface coating (surface-active agent).

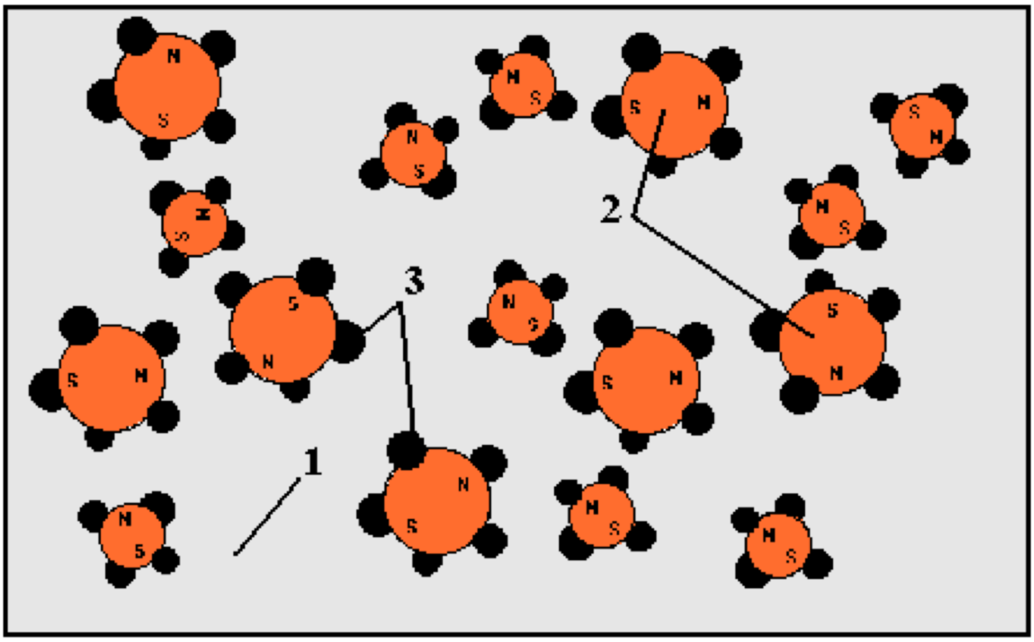

Figure 3. The structure of a magnetic liquid in the absence of a magnetic field.

The liquid carrier is based on mineral oil or water, kerosene, hydrocarbon or hydrofluoric liquids, esters or diesters. In general, the ferromagnetic materials are small particles of iron, cobalt, nickel and iron oxides. These micromagnets are colloidal, suspended in a magnetic or electrical carrier fluid. Principally, the attractive Van der Waals and magnetic forces, involved in nanoparticle collisions, have the ability to achieve gradual demagnetization.

Likewise, nanoparticles and dry suspensions lead to agglomeration due to the presence of Van der Waals forces and magnetic forces forming large clusters, for which the sedimentation rate cannot be counteracted by Brownian motion.

As a result, the ferromagnetic microparticles are covered with surface-active agents, e.g., oleic acid, to avoid aggregation and contribute to their stability. The fluid viscosity exhibits large reversible changes under a magnetic field. MR fluids have higher apparent viscosity and yield stress with an increasing magnetic field. Following the application of an external magnetic field, a fast variation in viscosity is exhibited. Magnetic fluids include MR fluids and ferrofluids.

The MR viscosity properties depend on the magnetic field and, hence, control the different high-dynamics application systems.

In the absence of an external magnetic field, the magnetic moments associated with each of the liquid particles are randomly oriented, and the resultant magnetic force vector is zero. After the application of an external magnetic field, the magnetic moments of the particles are arranged along the magnetic field force lines, forming chains, without surrendering to thermal movement (see Figure 4).

A small variation in the applied magnetic field causes strong changes in the liquid viscosity. Under an induced magnetic field, the viscosity of a liquid changes greatly. Generally, a greater B-field strength and chain stress induce greater viscosity in the fluid. The viscosity changes related to magnetic field variations occur in the order of milliseconds.

Magnetic liquids are classified as non-Newtonian liquids and can be well described using the Bingham constitutive model [43]:

$$\tau = \tau_0(B) + \mu \cdot \gamma \tag{7}$$

where τ is the shear stress in the fluid, $\tau_0(B)$ is the limit stress induced by a magnetic field with induction B, μ is the Newton dynamic viscosity of the liquid independent of the magnetic field and γ is the shear strain rate. In Figure 5, we show the relationship between the shear stress and strain rate, as described in Equation (7).

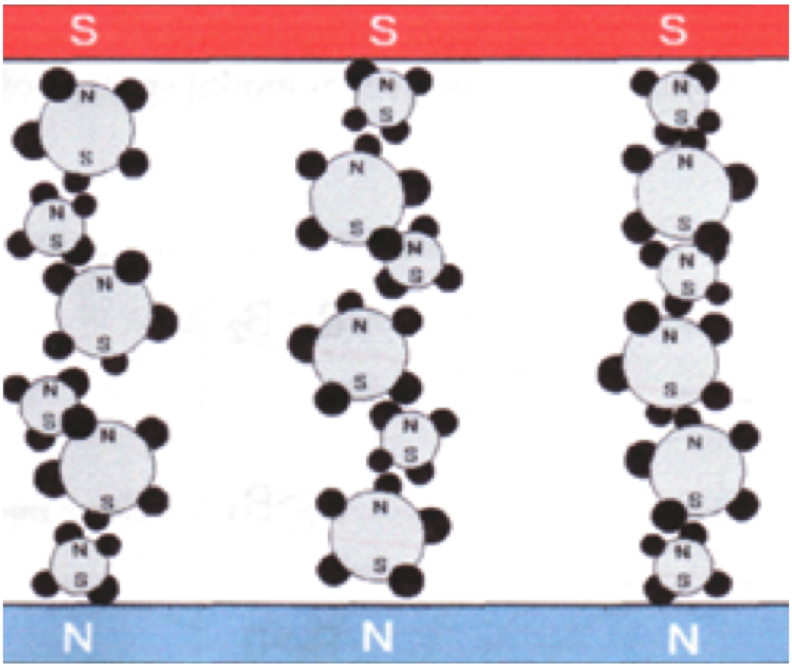

Figure 4. Magnetic particle distribution of an MR fluid with an external magnetic field.

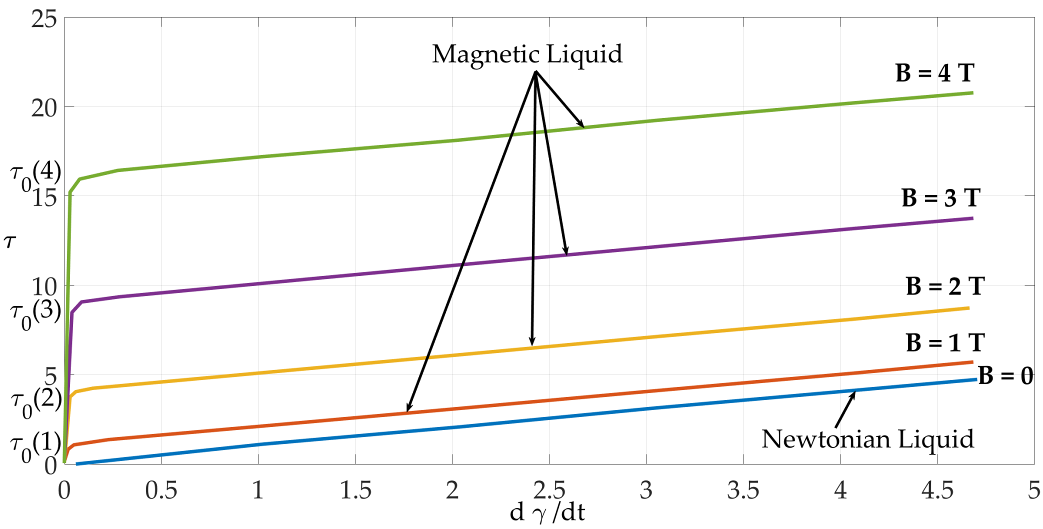

Figure 5. Dimensionless tangential stress versus dimensionless magnetic fluid deformation rate calculated as in [44] for $\mathbf{B} = 0$ compared with corresponding plots for $\mathbf{B} = 1, 2, 3, 4$ T.

The above equation holds for stresses τ greater than the stress limit $\tau_0(B)$. For stress values τ that are lower than the stress limit, the liquid behaves like an elastic body and Equation (7) must be replaced by the following equation:

$$\tau = G(B) \cdot \gamma \tag{8}$$

where $G(B)$ is the modulus of elasticity, dependent on magnetic induction.

Magnetic liquids depend on parameters such as the temperature. Currently, the produced liquids are characterized by good stability in terms of their properties as a function of the temperature. The basic viscosity of the liquid slightly decreases with an increasing temperature. Moreover, its magnetic permeability shows a very small decrease with an increasing temperature.

Magnetic fluids are distinguished as nanomagnetorheological fluids (ferrofluids) and micromagnetorheological fluids (MR). However, unlike ferromagnetic solids, ferrofluids do not exhibit hysteresis or residual magnetization once the magnetic field is removed due to thermal agitation.

Upon introducing a magnetic field, each particle behaves like a small permanent magnet, making it possible to control the macroscopic characteristics of the iron–fluid drops, such as the shape, viscosity, motion, etc.

For large particles inside ferrofluids, the viscosity change is based on the opposition to the free rotation of the particles: in the absence of a magnetic field, the dipole moments of the particles are randomly arranged, leaving them free to rotate. Upon introducing a field and consequently a privileged direction in space, the particles align with their dipole moments parallel to it.

Thermal agitation and viscous friction caused by motion apply a mechanical moment to each particle that tends to rotate them. This rotation is hampered by the magnetic torque that occurs when the dipoles are misaligned, leading to a macroscopic change in the viscosity of the liquid.

4. Experimental Set-Up

4.1. Experimental Tests

The experimental test equipment used includes the following main components (see Figure 1):

- measuring equipment;
- a variable AC transformer;
- an ammeter and a voltmeter;
- a two-channel oscilloscope.

An autotransformer is used to provide the power supply to the excitation coil and its working frequency is 50 Hz.

To create the magnetic field around the coil, the excitation has a required input voltage V_1 of 220 Volts; the output voltage V_2 varies in the range $0 \leq V_2 \leq 250$ [V]; and the maximum current I_{max} is 2.5 A.

The Tektronix MDO3012 mixed-domain oscilloscope (TEKTRONIX Manufacturer, Shanghai, China) has been integrated into the measurement system, connected directly to the excitation coils, for the ability to capture the voltage and current signals.

The type of hydrocarbon-based MR fluid used in the experimental tests is MRF-132DG, shown in Figure 6, produced by the LORD Corporation, Cary, NC, USA. Its properties are listed in Table 1.

Table 1. The main properties of MRF-132DG.

Typical Properties	MRF-132DG
Appearance	dark gray liquid
Viscosity Pa-s@40 °C (104 °F) calculated as slope 800–1200 s^{-1}	0.092 ± 0.015
Density g/cm^3	2.98–3.18
Operating Temperature °C	-40 to $+130$

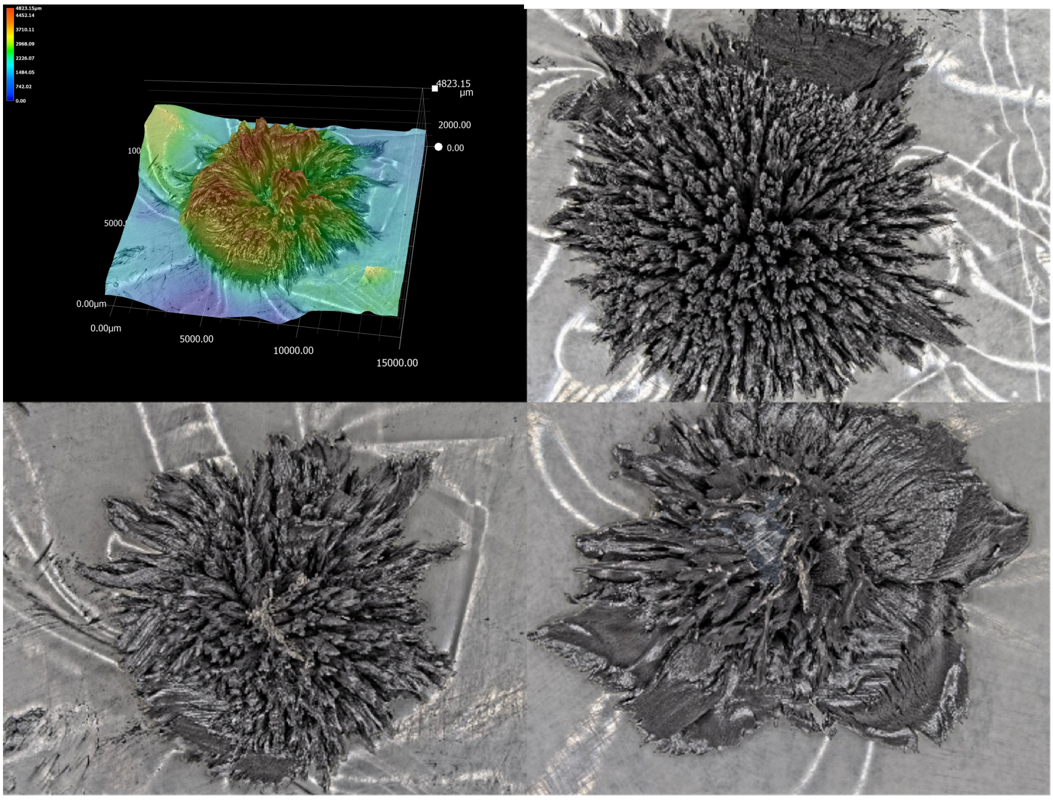

Figure 6. MR fluid MRF-132DG under a digital microscope, Keyence VHX-7000, Keyence Corporation, Osaka, Japan.

4.2. Devices and Materials

The experimental set-up for the measurement of the magnetic permeability of a magnetic fluid is composed of a container for the magnetic fluid, measuring coils, an excitation coil and a ferromagnetic core that forms a closed magnetic circuit (see Figure 7). The coils of the measuring device are structured as follows: the excitation coil surrounds the measuring coils and the magnetic liquid container; the first measuring coil is placed around the magnetic liquid container; and the second measuring coil is placed inside the excitation coil (see Figure 8).

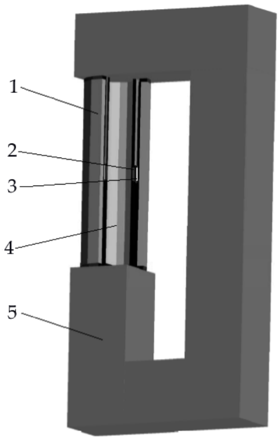

Figure 7. Measuring device: 1—core, 2—magnetic liquid, 3—receiving coils, 4—excitation coil, 5—apparatus block

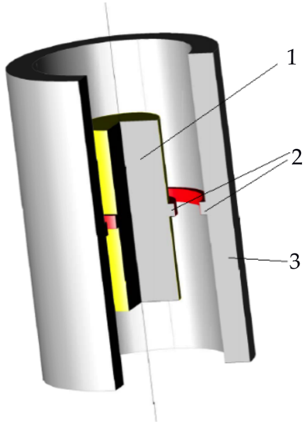

Figure 8. Coil system: 1—magnetic liquid, 2—receiving coils, 3—excitation coil.

The magnetic flux Φ_g is generated by the excitation coil, composed of a copper wire wrapped around a cylindrical former composed of polylactic acid (PLA), where the MR fluid is contained.

The magnetic flux Φ_g is a measurement of the total magnetic field that travels through the MR liquid container (Φ_M) and the surrounding air (Φ_δ).

4.3. Mathematical Model of Measuring Device

The measuring device works on the principle of measuring the voltage in two receiving coils. The induced voltages are related to the permeability. A mathematical model is provided in order to deliver the working principle of the device (see Figure 9). In the presented measuring device, the current flows through the coils and produces the magnetic flux. The coils of the magnetic structure can be considered in an interconnection that exhibits a network combination of parallel/series magnetic reluctance, as shown in Figure 9. The magnetic reluctance is defined as the ratio of the magnetomotive force to the magnetic flux and depends on the material properties and the geometry, i.e., the core material's length, area and permeability, as analogous to the resistance in the electric circuit. The reluctance is measured in the coil with an air gap and in magnetic materials. In this magnetic circuit, the magnetic material is combined with the air gap, as shown in Figure 9. In this magnetic circuit, reluctances are considered as resistances connected in parallel. The magnetic flux is analogous to the electric current. Therefore, we apply the equation of Kirchhoff's current law to the nodes of the circuit, with the current direction arrows chosen as in Figure 9, and a current divider is used for its ability to divide the total current into fractional parts. The magnetic flux relationship is described by the following equation:

$$\Phi_M = \Phi_g - \Phi_\delta \tag{9}$$

where the total magnetic flux Φ_g = Φ_M + Φ_δ is divided into an electrical current in the nodes of the circuit, Φ_M is the magnetic flux density of the MR and Φ_δ is the magnetic flux density in the surrounding air.

The following Equations (10) and (11) refer to the equivalent parallel circuit of the current divider, in which the current is divided into each branch. In a parallel connected circuit, the magnetic flux density through each resistor—in our case, the reluctance—in the parallel circuit is given by

$$\Phi_M = \frac{R_\delta}{R_\delta + R_M}\Phi_g \tag{10}$$

$$\Phi_\delta = \frac{R_M}{R_\delta + R_M}\Phi_g \tag{11}$$

Assume that R_δ is the reluctance of the air and R_M is the reluctance of the magnetic fluid. The reluctance depends on the geometrical and material properties of the circuit, and it is proportional to its length and inversely proportional to its cross-sectional area and magnetic permeability.

$$R_\delta = \frac{l}{S_\delta \cdot \mu_0} \tag{12}$$

and

$$R_M = \frac{l}{S_M \cdot \mu_M \cdot \mu_0} \tag{13}$$

where the coil is characterized by the length l, its cross-sectional area S_M outside the MR fluid container and its cross-sectional area S_δ in the air; μ_M is the magnetic permeability of the MR; and μ_0 is the magnetic permeability in the air.

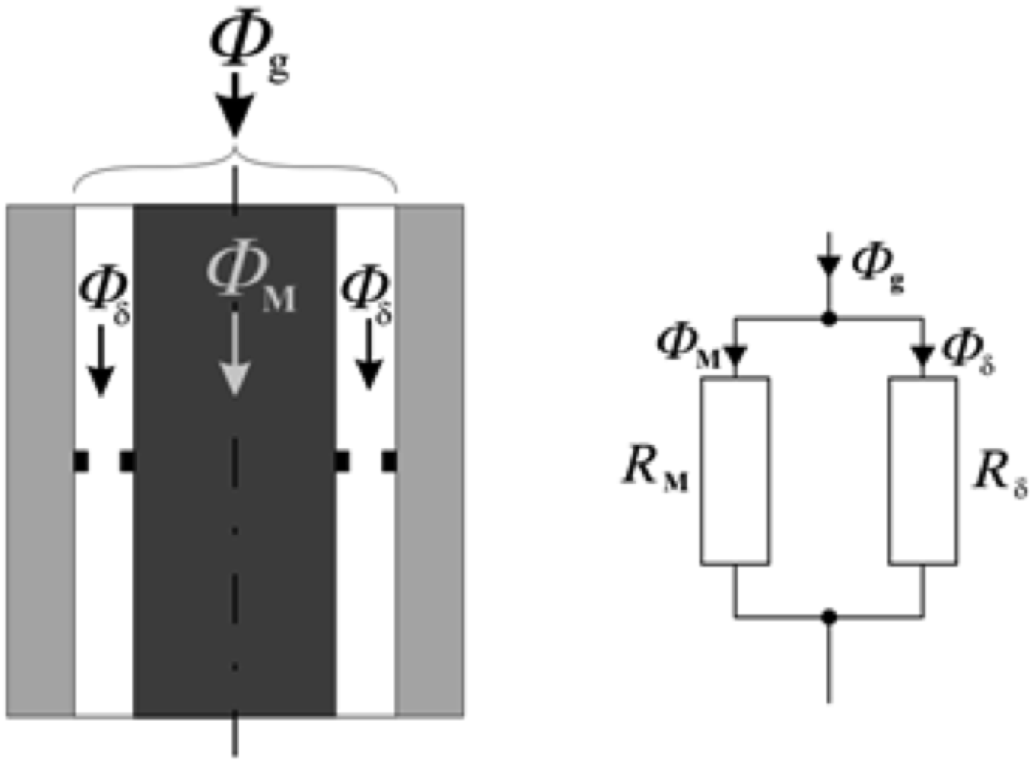

Figure 9. Magnetic flux flow inside the excitation coil.

By expressing Equations (10)–(13) in terms of the quantities that characterize the device, applying the algebraic equations, we obtain

$$\frac{\Phi_M}{\Phi_\delta} = \frac{R_\delta}{R_M} = \frac{\frac{l}{S_\delta \cdot \mu_0}}{\frac{l}{S_M \cdot \mu_M \cdot \mu_0}} = \frac{S_M \cdot \mu_M}{S_\delta} = \mu_M \cdot \frac{S_M}{S_\delta} \tag{14}$$

For the measuring device used, $S_M/S_\delta \approx 1$; then,

$$\mu_M = \frac{\Phi_M}{\Phi_\delta} \tag{15}$$

so that [45]

$$\mu_M = \frac{V_M}{V_\delta} \tag{16}$$

In Equation (16), V_1 is the induced voltage in the MR fluid cylinder, and V_2 is the voltage measured across the coil air coat. We have

$$V_\delta = V_2 - V_1$$
$$V_M = V_1$$

The following is a possible expression of Equation (16):

$$\mu_M = \frac{V_1}{V_2 - V_2} \tag{17}$$

As for the magnetic field within the coil system (B-field), it can be expressed as

$$B = \frac{V}{\frac{2\pi}{\sqrt{2}} \cdot N \cdot f \cdot \left(\frac{\pi \cdot \delta^2}{4} \right)} \tag{18}$$

where f is the operating frequency, N is the number of turns and δ is the radius of the cylinder coil.

Specifically,

$$\delta = 22 \text{ mm},$$
$$N = 400,$$
$$f = 50 \text{ Hz},$$
$$V = \frac{V_2}{2\sqrt{2}}$$

as the magnetic flux travels through the MR fluid and air coating of the coil system.

4.4. MR Fluid Permeability and MR Fluid Permeability

At the high or low excitation intensity of the magnetic field, the MR fluid responds immediately by amplifying or attenuating the field, satisfying different requirements in many engineering applications, such as in vehicle suspension and dampers, which resist motion via viscous friction.

The connection between the coil system and the autotransformer by electrical cables allows us to vary the voltage and the current in the range of 0 to 2 A with steps of 0.05 A. It also allows us to measure the voltages of the inducted magnetic fluxes with an oscilloscope, in which V_1 is the induced voltage caused by the magnetic field flux Φ_{MR}, and V_2 is the induced voltage due to the magnetic field flux through the air coating of the coil $(\Phi_{air\,coat} + \Phi_{MR})$).

The measurement time, namely the registration time, must be as short as possible. During the measurements, the set value of the supply voltage for the excitation coil was determined and the magnetization current was measured. The measurements were conducted in a very short time to avoid the heating of the coils (Figure 10).

The analytical function $\mu_r = f(B)$ is obtained as a linear combination of the Gabor system elements generated by a Gaussian function $\phi(t) = e^{-t^2}$ by means of the translation and scaling of the generating function [46] using the experimental dataset:

$$\mu_r = \sum_{i=1} c_i \cdot G_{\sigma_i}(B) * \delta(B - \mu_i) \tag{19}$$

$*$ denotes the convolution operator, $\delta(B - \mu_i)$ is the Dirac function centered upon μ_i and

$$G_{\sigma_i}(B) = exp\left(-\frac{B^2}{2\sigma_i^2} \right)$$

The coefficients c_i, σ_i, μ_i can be calculated by using the pseudo-inverse operator, but this implies numerical instabilities. Thus, to reduce the computations required, the mathematical expression $\mu_r = f(B)$ is calculated by means of a radial basis function neural network [47–49].

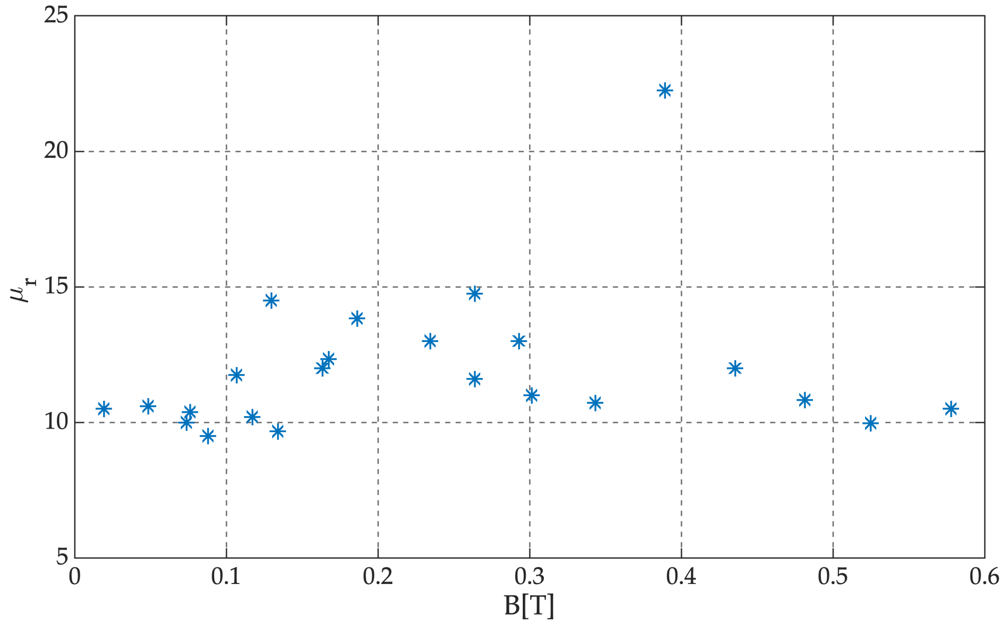

Figure 10. Measured MR fluids' relative magnetic permeability as function of magnetic intensity

5. Results

Experimental Results and Neural Modeling

It is well known that Gaussian RBF neural networks are capable of uniformly approximating arbitrary continuous functions defined on a compact set to satisfy a given approximation error. This approximation process is usually carried out in a learning phase where the number of hidden nodes and the network parameters are appropriately adjusted so that the approximation error is minimized.

The developed RBF neural network model consists of three layers: an input layer, a hidden layer and an output layer. The type of transfer function is a Gaussian function for the hidden layer, and the third layer, corresponding to the output layer, has one neuron with a linear transfer function.

For RBFs, it is necessary to determine the weights and the radii σ_i using the backpropagation algorithm and the set of bump locations μ_i via the k-means algorithm.

The Gaussian function is used for the radial basis function, expressed as in Equation (20):

$$\phi(t) = e^{-\left(\frac{r}{\sigma}\right)^2} \tag{20}$$

The radii σ_i are set to equal values using the simple heuristic function

$$\sigma_i = \frac{d_{max}}{\sqrt{2m}} \tag{21}$$

where d_{max} is the maximum distance between the selected data inputs, and m is the number of data in the training set.

Then, the weights are calculated, as well as the radii and center vectors, by iteratively computing the partials and performing the following updates:

$$\begin{gathered} E = \frac{1}{2}\sum_{j=1}^{m}(d_j - y_j)^2 = \frac{1}{2}\sum_{j=1}^{m} e_j^2 \\ w_{i,j}^{new} = w_{i,j}^{old} - \eta_1 \frac{\partial E}{\partial w_{i,j}} \end{gathered} \tag{22}$$

where η_1 are learning rate coefficients.

The training dataset consists of input vectors containing the measured B-field strength and the target output containing the measured relative magnetic permeability. The training dataset includes 350 samples of laboratory measurements of the magnetic B-field and the relative magnetic permeability. The test data include 65 samples, used for the generalization of the neural network.

The preliminary selection of the centers for the Gaussian functions is carried out by randomly selecting 285 data from the training set. As soon as the clustering algorithm is complete, the parameters are adjusted by using Equations (21) and (22). These parameters control the amount of overlapping of the radial basis functions, as well as the network generalization. A small value of overlap yields a rapidly decreasing function, while a large value results in a more gradually varying function. In order to achieve better generalization, after the abovementioned training step, a pruning procedure is applied in order to reduce the RBFs' complexity and eliminate redundant weights. The resulting network is retrained and subjected to the pruning procedure again. The training process ends quickly as the error has a tendency to increase [50,51]. Therefore, the analytical formula for μ_r after the pruning procedure is

$$\mu_r = 4.5 \cdot exp\left(-\frac{(B-0.23)^2}{0.072}\right) - exp\left(\frac{-(B-0.4)^2}{0.0373}\right) + 10.5$$

where the magnetic field strength is defined as a function of the measured relative permeability μ_r of the MR fluid, as shown in Figure 11. The results obtained show good agreement with the experimental investigation, with an error of roughly 8%.

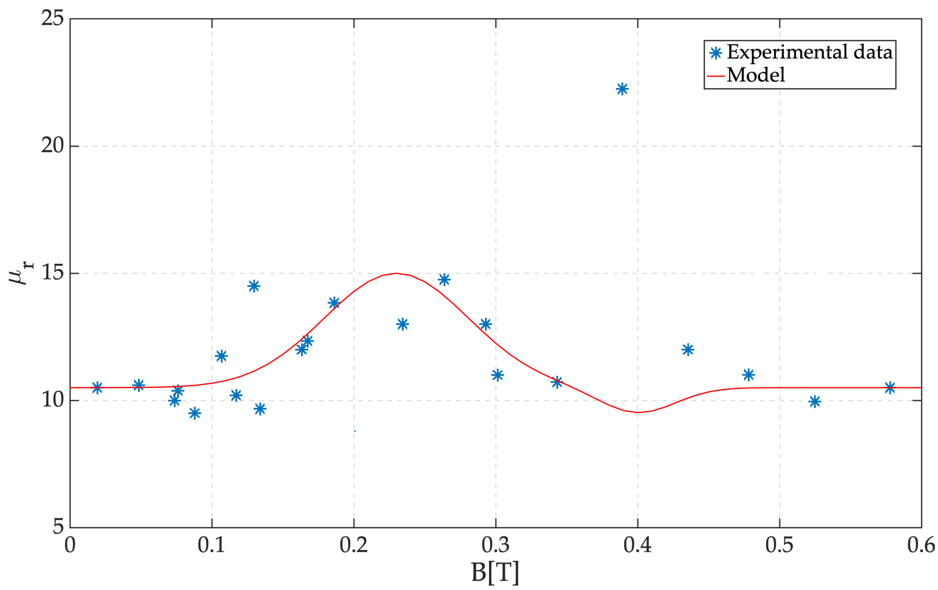

Figure 11. The measured μ_r of MR fluids and the simulated ones by the model obtained with RBFs.

6. Conclusions

Recently, the progress in materials technology and the important role of electronics in mechanical engineering have yielded significant progress in the production of electric vehicles and in the automotive industries. In particular, MR materials are of considerable significance in these areas.

Magnetorheological and electrorheological fluids are materials that manifest a change in rheological behavior when subjected, respectively, to a magnetic or electric field. For these materials, therefore, simple and accurate electrical/magnetic characterization is important.

In this research, an accurate model based on a small number of parameters is described, for which the relative magnetic permeability of the MR fluids is a function of the applied magnetic field. A new metering system is proposed for the magnetic characterisation of MR fluids.

Starting with the experimental data obtained in this way, the mathematical relation $\mu_r = f(B)$ is represented by means of a radial basis function neural network (RBF), with neurons having a Gaussian activation function. Then, the network is trained with the experimental data and a pruning procedure is applied. As a result, the defined mathematical relation $\mu_r = f(B)$ is in accordance with the experimental results, with an error of roughly 8%.

Author Contributions: Conceptualization, P.K. and G.L.S.; methodology, G.L.S., P.K., R.B. and G.C.; software, G.C.; validation, R.B., G.C., G.L.S. and P.K.; formal analysis, P.K.; investigation, G.L.S. All authors have read and agreed to the published version of the manuscript.

Funding: This research received no external funding.

Institutional Review Board Statement: Not applicable.

Informed Consent Statement: Not applicable.

Data Availability Statement: Data are contained within the article.

Conflicts of Interest: The authors declare no conflicts of interest.

References

1. Kowalewska, A.; Majewska-Smolarek, K. Synergistic Self-Healing Enhancement in Multifunctional Silicone Elastomers and Their Application in Smart Materials. *Polymers* **2024**, *16*, 487. [CrossRef]
2. De Schryver, R.; Jiao, D.; Yardimci, M.Y.; Lesage, K.; De Schutter, G. A conceptual model for numerical simulation of Active Rheology Control validated for cementitious pumping. *Cem. Concr. Res.* **2024**, *179*, 107471. [CrossRef]
3. Le, C.V.; Yoon, H. Advances in the Use of Conducting Polymers for Healthcare Monitoring. *Int. J. Mol. Sci.* **2024**, *25*, 1564. [CrossRef]
4. Caushaj, S.; Imberti, G.; de Carvalho Pinheiro, H.; Carello, M. Electromagnetic Interaction Model between an Electric Motor and a Magnetorheological Brake. *Designs* **2024**, *8*, 25. [CrossRef]
5. Ciulli, E. Vastness of Tribology Research Fields and Their Contribution to Sustainable Development. *Lubricants* **2024**, *12*, 33. [CrossRef]
6. Zhu, J.; Hu, H.; Zhao, W.; Yang, J.; Ouyang, Q. Design and Control of Upper Limb Rehabilitation Training Robot Based on a Magnetorheological Joint Damper. *Micromachines* **2024**, *15*, 301. [CrossRef]
7. Liu, Z.; Li, W.; Tan, X.; Huang, Y.; Tao, Y.; Yang, N.; Yuan, R.; Liu, L.; Ge, L. Transformable Magnetic Liquid-Metal Nanoplatform for Intracellular Drug Delivery and MR Imaging-Guided Microwave Thermochemotherapy. *ACS Appl. Mater. Interfaces* **2024**, *16*, 9826–9838. [CrossRef]
8. Hu, G.; Yi, F.; Tong, W.; Yu, L. Development and Evaluation of a MR Damper With Enhanced Effective Gap Lengths. *IEEE Access* **2020**, *8*, 156347–156361. [CrossRef]
9. Nordin, N.H.D.; Muthalif, A.G.A.; Razali, M.K.M.; Ali, A.; Salem, A.M. Development and Implementation of Energy-Efficient Magnetorheological Fluid Bypass Damper for Prosthetics Limbs Using a Fuzzy-Logic Controller. *IEEE Access* **2022**, *10*, 18978–18987. [CrossRef]
10. Hu, G.; Wu, L.; Li, L.; Yu, L. Performance Analysis of Rotary Magnetorheological Brake With Multiple Fluid Flow Channels. *IEEE Access* **2020**, *8*, 173323–173335. [CrossRef]
11. Dutra, R.M.A.; de Andrade, R.M.; Soares, A.B.; Thakor, N.V.; Vimieiro, C.B.S. Magnetorheological fluid in prostheses: A state-of-the-art review. *J. Intell. Mater. Syst. Struct.* **2024**, *35*, 1045389X231213126. [CrossRef]
12. Rajput, A.S.; Das, M.; Kapil, S. A Hybrid Electrochemical Magnetorheological Finishing Process for Surface Enhancement of Biomedical Implants. *J. Manuf. Sci. Eng.* **2024**, *146*, 051004. [CrossRef]
13. Chauhan, V.; Kumar, A.; Sham, R. Magnetorheological fluids: A comprehensive review. *Manuf. Rev.* **2024**, *11*, 6. [CrossRef]
14. Bai, X.X.; Chen, P. On the hysteresis mechanism of magnetorheological fluids. *Front. Mater.* **2019**, *6*, 36. [CrossRef]
15. Behera, S.K.; Sarangi, S. Constitutive modeling of electro-magneto-rheological fluids before yielding. *Mech. Res. Commun.* **2024**, *136*, 104253. [CrossRef]
16. Khajehsaeid, H.; Alaghehband, N.; Bavil, P. On the yield stress of magnetorheological fluids. *Chem. Eng. Sci.* **2022**, *256*, 117699. [CrossRef]
17. Wang, H.; Bi, C.; Liu, W.; Zhou, F. Squeeze behaviors of magnetorheological fluids under different compressive speeds. *Materials* **2023**, *16*, 3109. [CrossRef]
18. Kumar, J.S.; Paul, P.S.; Raghunathan, G.; Alex, D.G. A review of challenges and solutions in the preparation and use of magnetorheological fluids. *Int. J. Mech. Mater. Eng.* **2019**, *14*, 1–18. [CrossRef]

19. Wu, C.; Zhang, Q.; Fan, X.; Song, Y.; Zheng, Q. Smart magnetorheological elastomer peristaltic pump. *J. Intell. Mater. Syst. Struct.* **2019**, *30*, 1084–1093. [CrossRef]
20. Hafez, A.; Liu, Q.; Santamarina, J.C. Magneto-rheological fluids: Tele-manipulation of ferromagnetic particles with external magnetic field for flow control and zonal isolation. *Geoenergy Sci. Eng.* **2023**, *228*, 212029. [CrossRef]
21. Upadhyay, R.V.; Choi, S.B. Modeling, measurements and validation of magnetic field dependent flow behavior of magnetorheological fluids; static and dynamic yield stress. *Smart Mater. Struct.* **2021**, *30*, 117002. [CrossRef]
22. Dai, X.R.; Zhu, M. Frame set for Gabor systems with Haar window. *Appl. Comput. Harmon. Anal.* **2024**, *71*, 101655. [CrossRef]
23. Yarali, E.; Mohammadi, A.; Mafakheri, S.; Baghani, M.; Adibi, H. Mathematical modeling and experimental evaluation of a prototype double-tube Magnetorheological damper. *SN Appl. Sci.* **2019**, *1*, 1–10. [CrossRef]
24. Lin, H.; Dai, H.; Mao, Y.; Wang, L. An optimized radial basis function neural network with modulation-window activation function. *Soft Comput.* **2024**, *28*, 4631–4648. [CrossRef]
25. Lo Sciuto, G.; Capizzi, G.; Shikler, R.; Napoli, C. Organic solar cells defects classification by using a new feature extraction algorithm and an EBNN with an innovative pruning algorithm. *Int. J. Intell. Syst.* **2021**, *36*, 2443–2464. [CrossRef]
26. Lo Sciuto, G.; Napoli, C.; Capizzi, G.; Shikler, R. Organic solar cells defects detection by means of an elliptical basis neural network and a new feature extraction technique. *Optik* **2019**, *194*, 163038. [CrossRef]
27. Liu, S.; Yu, G.; Kim, Y. Supplier Evaluation in Supply Chain Environment Based on Radial Basis Function Neural Network. *Int. J. Inf. Technol. Web Eng. (IJITWE)* **2024**, *19*, 1–18. [CrossRef]
28. Singh, R.; Srivastava, A.; Kant, R.; Maurya, S.; Mahadasu, P.; Verma, N.; Hema, G.; Kushwaha, P.; Richa.; Singh, K.; et al. Integrated thin layer classification and reservoir characterization using sparse layer reflectivity inversion and radial basis function neural network: A case study. *Mar. Geophys. Res.* **2024**, *45*, 3. [CrossRef]
29. Taoufyq, E.; Mohammed, O.; Hamid, B. Multi-objective optimization of radial basis function neural network training using genetic algorithm. *AIP Conf. Proc.* **2024**, *3034*, 020001.
30. Stanišić, D.; Mejić, L.; Jorgovanović, B.; Ilić, V.; Jorgovanović, N. An Algorithm for Soft Sensor Development for a Class of Processes with Distinct Operating Conditions. *Sensors* **2024**, *24*, 1948. [CrossRef]
31. Zahir, H.; Gul, J.; Inc, M.; Alqahtani, R.T. Impact of fractional magnetohydrodynamic and hall current on ree-eyring fluid flow by using radial basis function method. *Alex. Eng. J.* **2024**, *88*, 210–215. [CrossRef]
32. Yang, X.; Chen, W.; Yin, C.; Cheng, Q. Fractional-Order Sliding-Mode Control and Radial Basis Function Neural Network Adaptive Damping Passivity-Based Control with Application to Modular Multilevel Converters. *Energies* **2024**, *17*, 580. [CrossRef]
33. Moezi, S.A.; Sedaghati, R.; Rakheja, S. Nonlinear dynamic modeling and model-based AI-driven control of a magnetoactive soft continuum robot in a fluidic environment. *ISA Trans.* **2024**, *144*, 245–259. [CrossRef]
34. Zheng, J.; Chen, S.; Xiao, Y. Effective permeability model of magnetorheological fluids and its experimental verification. *J. Magn. Magn. Mater.* **2022**, *562*, 169774. [CrossRef]
35. Bi, C.; Bi, E.; Wang, H.; Deng, C.; Chen, H.; Wang, Y. Magnetic circuit design for the performance experiment of shear yield stress enhanced by compression of magnetorheological fluids. *Sci. Rep.* **2024**, *14*, 741. [CrossRef]
36. Li, Z.; Fu, B.; Liao, C. Impact behavior of a novel magnetorheological energy absorber based on wedge-shaped squeeze flow model. *J. Intell. Mater. Syst. Struct.* **2024**, *35*, 1045389X231220796. [CrossRef]
37. Kubík, M.; Žáček, J.; Gołdasz, J.; Nečas, D.; Sedlačík, M.; Blahuta, J.; Bańkosz, W.; Sapiński, B. Grasping the behavior of magnetorheological fluids in gradient pinch mode via microscopic imaging. *Phys. Fluids* **2024**, *36*,042004. [CrossRef]
38. Yu, B.; Ma, J.; Zhao, X.; Chen, Y. Numerical simulation for microstructure evolution of magnetorheological fluid based on combined disk DDA-LBM approach. *Powder Technol.* **2024**, *437*, 119585. [CrossRef]
39. Alimisis, V.; Dimas, C.; Sotiriadis, P.P. A Low-Power Analog Integrated Euclidean Distance Radial Basis Function Classifier. *Electronics* **2024**, *13*, 921. [CrossRef]
40. Stenkin, D.; Gorbachenko, V. Mathematical Modeling on a Physics-Informed Radial Basis Function Network. *Mathematics* **2024**, *12*, 241. [CrossRef]
41. Lang, Q.; Lu, J. Learning Memory Kernels in Generalized Langevin Equations. *arXiv* **2024**, arXiv:2402.11705.
42. Galushkin, A.I. *Neural Networks Theory*; Springer Science & Business Media: Berlin/Heidelberg, Germany, 2007.
43. Fedorowicz, K.; Prosser, R. The elastic perfectly plastic constitutive equation for yield stress fluids. *J. Non-Newton. Fluid Mech.* **2024**, *352*, 105201. [CrossRef]
44. Feng, Z.; Zhang, Z.; Yang, J.; Yu, J.; Feng, J.; Zhou, H.; Shi, C.; Meng, F. Advanced nonlinear rheology magnetorheological finishing: A review. *Chin. J. Aeronaut.* **2023**, *37*, 54–92.
45. Kowol, P.; Pilśniak, A.; Zioło, G.; Lo Sciuto, G. Stanowisko do badania przenikalności magnetycznej cieczy magnetoreologicznej. *Pomiary Autom. Robot.* **2020**, *24*, 11–17.
46. Dong, X.; Rudelson, M. Approximately Hadamard matrices and Riesz bases in random frames. *Int. Math. Res. Not.* **2024**, *2024*, 2044–2065. [CrossRef]
47. Loh, C.H.; Chen, Y.C.; Su, C.T. Using Transfer Learning and Radial Basis Function Deep Neural Network Feature Extraction to Upgrade Existing Product Fault Detection Systems for Industry 4.0: A Case Study of a Spring Factory. *Appl. Sci.* **2024**, *14*, 2913. [CrossRef]
48. Song, S.; Wang, P.; Heidari, A.A.; Zhao, X.; Chen, H. Adaptive Harris hawks optimization with persistent trigonometric differences for photovoltaic model parameter extraction. *Eng. Appl. Artif. Intell.* **2022**, *109*, 104608. [CrossRef]

49. Fernández, J.; Chiachío, M.; Chiachío, J.; Muñoz, R.; Herrera, F. Uncertainty quantification in Neural Networks by Approximate Bayesian Computation: Application to fatigue in composite materials. *Eng. Appl. Artif. Intell.* **2022**, *107*, 104511. [CrossRef]
50. Tan, Y.; Liu, H. How does a kernel based on gradients of infinite-width neural networks come to be widely used: A review of the neural tangent kernel. *Int. J. Multimed. Inf. Retr.* **2024**, *13*, 8. [CrossRef]
51. Lazovskiy, N.V. Neural Network System for Monitoring the Condition of Equipment and Predicting Malfunctions. In Proceedings of the 2024 Conference of Young Researchers in Electrical and Electronic Engineering (ElCon), St. Petersburg, Russia, 29–31 January 2024; IEEE: Piscataway, NJ, USA, 2024; pp. 421–423.